

Microstructural studies of electrospark deposited aluminide coatings on 9Cr steels

N. I. Jamnapara^{*1,2}, S. Frangini³, D. U. Avtani¹, V. S. Nayak¹, N. L. Chauhan¹, G. Jhala¹, S. Mukherjee¹ and A. S. Khanna²

Electrospark deposition (ESD) technique has been used to apply an iron aluminide coating on 9Cr reduced activation steel, which is a structural material for test blanket modules of fusion reactors. Phase identification and microstructural analysis of the aluminide coating along with the interface region were performed with the support of X-ray diffraction technique, optical microscopy, scanning electron microscopy and nanoindentation hardness measurements. Microstructural examination indicated prominent changes in the near interface microstructure of the steels processed by the ESD process. The substrate side of the coating/substrate interface consisted of a soft zone that is possibly of quasi-amorphous nature and of an $M_{23}C_6$ type carbide segregation rich area below this interface. The coating, however, showed extensive crack defects that need to be removed for reliably assessing its suitability as a barrier layer for blanket applications.

Keywords: Electrospark deposition, Aluminide, Blanket, 9Cr Steels

Introduction

Reduced activation 9Cr ferritic steels (RAFMSs) are currently under intense consideration as basic structural materials for blanket module testing in fusion reactors.^{1,2} The test blanket modules of the fusion reactor have to generate tritium, which is the fuel for the fusion reactor, by absorbing 14 MeV neutrons and transforming their energy into heat, which is then transferred to a coolant to generate electricity.² The Indian test blanket module uses both solid and liquid breeder concepts.³ Critical issues with the liquid breeder material, i.e. eutectic Pb–17Li operating at 320–480°C, are: corrosion of structural material (RAFMS), tritium permeation into RAFMS and magnetohydrodynamic drag generation due to flowing Pb–17Li.⁴ In order to mitigate these issues, an insulator coating such as Al_2O_3 has been reported^{5,6} to offer better tritium permeation resistance and protection against Pb–17Li attack, besides providing electrical insulation. However, the large difference in the coefficient of thermal expansion (CTE) between the Al_2O_3 coating and the steel leads to cracks and spalling, which does not make it eligible alone as a suitable coating.⁶ Further studies point out that an intermediate layer such as FeAl type iron–aluminide alloy could mitigate the CTE difference and also would act as a reservoir for Al, thus providing a basis for a self-healing Al_2O_3 coating system.⁷ Based on these premises, aluminide coatings are nowadays

the first choice candidates to protect such 9Cr steels against tritium permeation and molten metal attack by Pb–15·7Li eutectic tritium breeder liquids.^{8,9} To date, various coating techniques, namely chemical vapour deposition, hot dip aluminising (HDA), vacuum plasma spray and electrochemical deposition, have been tested^{9,10} with variable results. It remains also an open question whether the aluminising process must be applied before the fabrication process or vice versa. In the event of welding aluminised components, even the weld joint will be required to be sealed with the aluminised layer to provide complete protection to the blanket module. No work has been reported to date on this issue, although efforts to investigate a process to coat weld zones are of valuable interest. In this context, a new technique called electrospark deposition (ESD) process is being explored here. The ESD is a novel surfacing technique that uses a rotating electrode to deposit microweld coating with a very low heat input. The ESD technique is best suited for small and selected area application on high precision components. This technique has been very recently used by one of the authors¹¹ for applying corrosion resistant aluminide coatings on high temperature fuel cell stainless steel materials. The low heat transfer and the diffusion coating nature are two desirable properties of the ESD processing that could be advantageously exploited for coating welded areas of 9Cr reduced activation steels. However, to the best of our knowledge, this technique has never been applied before for treating 9Cr ferritic–martensitic steel substrates. Pure FeAl instead of Al has been considered as the material of coating in this work since Al would further require diffusion heat treatment to convert it into FeAl, which may alter the properties of the substrate. On the other hand, FeAl is well known for its high temperature stability and oxidation resistance,¹² thus providing the

¹FCIPT Division, Institute for Plasma Research, Gandhinagar 382016, India

²Department of Metallurgical Engineering and Materials Science, IIT Bombay, Powai, Mumbai 400076, India

³Department UTRINN-IFC, ENEA CR Casaccia, Rome 00123, Italy

*Corresponding author, email nirav@ipr.res.in

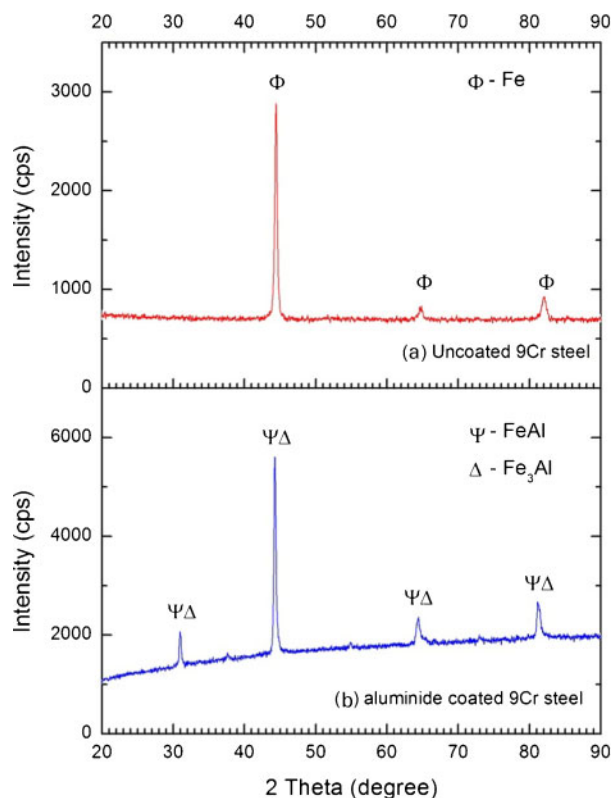
most desired phase in HDA treatments.¹³ On high temperature exposure in the presence of oxygen, FeAl forms a protective Al_2O_3 film on the surface, which makes it a self-healing coating.^{12,13} Since Pb–17Li eutectic liquid is expected to have 1300 ppm of oxygen content,¹⁴ FeAl would form a protective Al_2O_3 film. Keeping in view the above conditions, coating of FeAl by ESD process on welded zones is being explored. However, a preliminary analysis of the effect of such FeAl coating by ESD on the substrate and interface properties is felt as important to evaluate the acceptability of this process for nuclear coating applications. Consequently, this paper reports the microstructural study of low activation 9Cr steels post-aluminisation treatment by ESD.

Experimental

Reduced activation 9Cr steel samples mainly comprising of 9.05 wt-%Cr and 1.06 wt-%W in normalised and tempered condition were cut and mirror polished. These 9Cr steel samples were surface treated with a stoichiometric iron aluminide alloy filler rod (5 mm diameter) containing 24.4 wt-%Al. In detail, the coatings were applied using a commercial ESD handheld coating system (SparkDepo™ machine, model 28-40 by TechnoCoat, Japan) under argon gas shielding. Heat build-up on the treated areas was minimised using an Exair Cold Gun™ gas coolant system that kept the substrate temperature $<50^\circ\text{C}$. The following ESD processing parameters were used: 1300 W pulse power, 144 μs pulse length, 3000 rev min^{-1} electrode rotating speed and 400 Hz repetition pulse frequency. The contact force parameter was also controlled according to the procedures described in Ref. 15. The average contact force was kept in the range 0.1–0.5 N. Repetition deposition cycles were used to ensure high uniformity and coating continuity surfaces. In order to remove some gross deposit spatters, a final finishing treatment was also carried out with the same above processing parameters except that air shielding was used in this case to promote much higher substrate heating ($>100^\circ\text{C}$), resulting in prevalent substrate erosion effects. Based on the overall amount of material deposited on the sample surface area (14 cm^2), the maximum coating thickness was estimated at around 40–50 μm .

These samples were then cut using a diamond wafer blade, and the cross-section was mirror polished as per ASTM E3-01. The polished samples were etched using 4% nital solution as per standard etching practice specified in ASTM E407 and subjected to heat tinting technique. The heat tinting was chosen since it forms a thin oxide film on the surface, which leads to phase discrimination in optical microscopy.¹⁶ In order to study the phase changes in the microstructure of the ESD coating, heat tinting was performed on the coated samples. Heat tinting with 4% nital etching of samples involved exposure to 260°C for 1 h for effective identification of prior austenite grains and carbides in the matrix microstructure.

Various characterisation techniques were employed for microstructure and composition analysis. X-ray diffraction (XRD) studies were carried out using a PanAnalytical X-ray diffractometer (model X'Pert powder) with Cu K_α radiation ($\lambda=1.5406 \text{ \AA}$ and $2\theta=20\text{--}90^\circ$) in powder mode. Metallographic cross-sections of the aluminised 9Cr steel samples were studied with a Leica



1 Powder XRD pattern of a 9Cr steel sample in uncoated, normalised and tempered condition and b ESD aluminide coated 9Cr steel sample

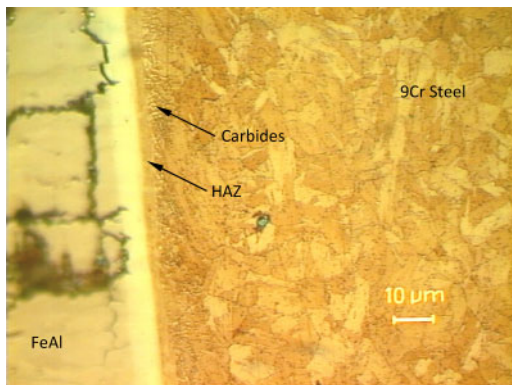
optical metallurgical microscope (model DMRM). Heat tinting as described earlier was carried out on the etched samples to bring optimal contrast images. The etched 9Cr steel aluminised samples were also studied with an LEO scanning electron microscope (SEM) (model: s440i; LEO Corporation) equipped with energy dispersive X-ray (EDX) technique for elemental analysis.

Nanoindentation measurements were performed at various sample locations on the heat tinted cross-section. Nanoindentation tests were carried out using Hystiron Inc., USA nanoindenter (model TI 900) with a Berkovich tip. Hardness numbers were obtained by applying a 3 mN load with a total cycle time of 30 s (loading time 10 s + dwell time 10 s + unloading time 10 s).

Results and discussion

X-ray diffraction analysis

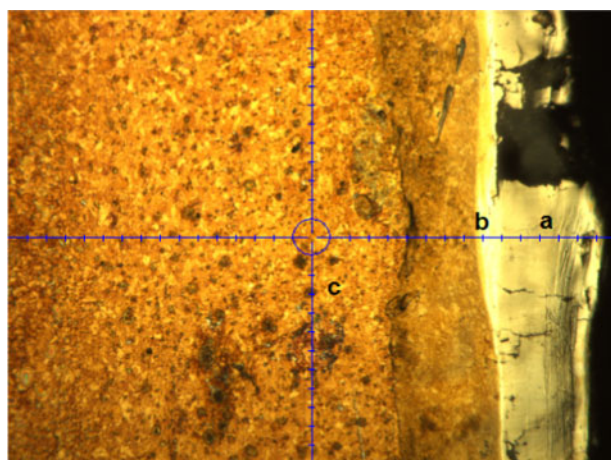
The XRD patterns observed on bare 9Cr steel and aluminide coated 9Cr steel samples are given in Fig. 1. The XRD pattern for bare steel conforms to the Fe–Cr alloy standard (as per International Centre for Diffraction Data file 35-1375), while the ESD coated 9Cr steel indicates the presence of FeAl phase (as per International Centre for Diffraction Data file 33-0020). Though the filler material consisted exclusively of FeAl phase, it is unclear from the XRD profiles whether the coating might also have some quantities of Fe_3Al phase,¹⁷ and hence, both FeAl and Fe_3Al are indicated in the XRD plot as possible phases.



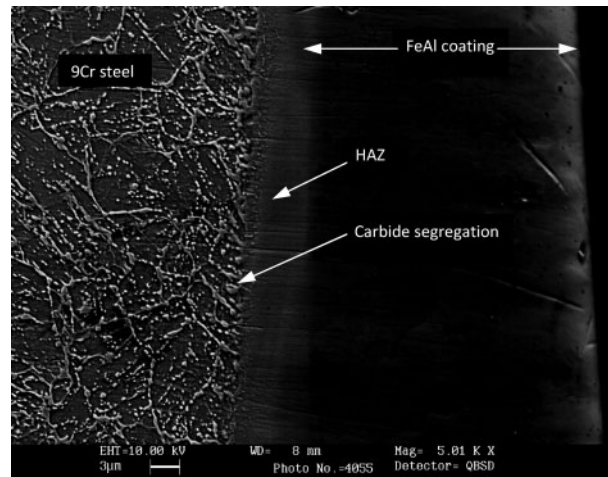
2 Heat tinted cross-section optical microstructure of ESD aluminised 9Cr steel

Optical microscopy

The optical microstructure at the coating/substrate interface is shown in Fig. 2. The presence of a shallow heat affected zone (HAZ) induced by ESD treatment is also clearly visible. The HAZ is composed of a sandwich layer below the coating. Upon close observation of Fig. 2, it can be seen that the area indicated as 'HAZ' below the bright interface does not show any grain boundary but has been tinted due to etching similar to the tint of the substrate. This indicates that the 'tinted area' indicated as 'HAZ' in Fig. 2 could be of base material (9Cr steel) but without any grain boundaries. Sections on 'Scanning electron microscope-EDX analysis' and 'Nanoindentation measurements' give more details on the nature of this zone. The substrate area below this bright layer is characterised by some grain refinement and carbide segregation. The core microstructure is formed of prior austenite grains of $\sim 6 \mu\text{m}$ size, while tempered martensite laths supposed to be present within the prior austenite grains are not clearly visible in the optical micrograph except that in a few areas owing to the nature of nital etchant. However, with the help of the Schaeffler-Schneider diagram, prediction of martensite formation can be also made based on the steel composition.¹⁸ From the figure, it also appears that the aluminide coating developed mud crack patterns, which are indicative of the thermal cracking phenomena produced by ESD treatment. Thermal



3 Optical image indicating locations of nanoindentation at coating (zone 'a'), interface (zone 'b') and substrate (zone 'c')



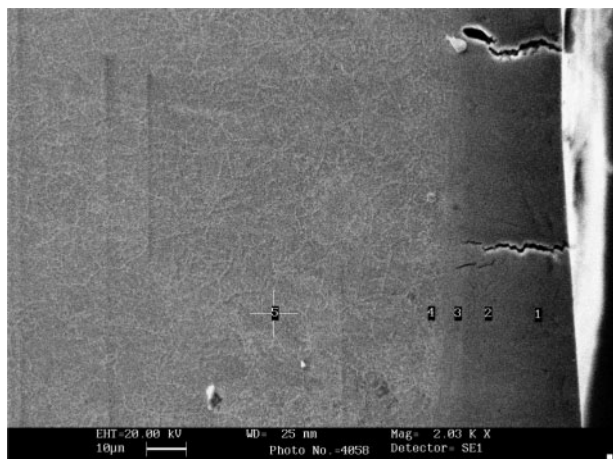
4 Back scattered cross-section SEM image of aluminised 9Cr steel

cracking arises because of the large mismatch in CTE between coating and substrate (namely $21 \times 10^{-6} \text{C}^{-1}$ for the FeAl phase¹⁹ and $12 \times 10^{-6} \text{C}^{-1}$ for the steel substrate²⁰ respectively). Since the CTE of FeAl materials is larger than that of steel substrate, coating shrinks much more than the substrate during cooling with consequent rapid build-up of tensile stresses inside the coating. At zones where such tensions exceed the material strength, vertical channel cracking develops. At the extremity of such cracks, some coating delamination may also take place, as evident in Fig. 3. However, it cannot be excluded that some coating defects are also introduced by metallographic preparation due to the brittle nature of iron aluminide materials. In any case, the cracking presence creates a necessity for more strict control of the ESD process conditions, namely steady contact force, constant work piece electrode distance, etc., for thermal effect minimisation. In one important aspect, preheating steps and/or post-coating treatments may be incorporated in the ESD processing in order to minimise residual stress defects from high cooling rates. For instance, it has been recently demonstrated that the ESD coating quality can be improved by applying post-deposition laser treatments capable to increase the surface smoothness and at the same time reduce coating porosity and cracking defects.^{21,22}

Scanning electron microscopy and EDX analysis

As a premise, heat tinting was found useful not only for optical microscopy observations but also for a fine structure analysis in SEM studies. Figure 4 shows a back scattered image of the heat tinted cross-section of the aluminised 9Cr steel sample with a focus on the interface. The image indicates a coating thickness of $\sim 32 \mu\text{m}$ with some cracks in the coating. Under back scattering SEM examination, the bright interface as visible in the optical micrograph (Fig. 2) appears in a light grey contrast colour, thereby suggesting a significant change in the elemental composition of the interface zone with respect to the coating layer.

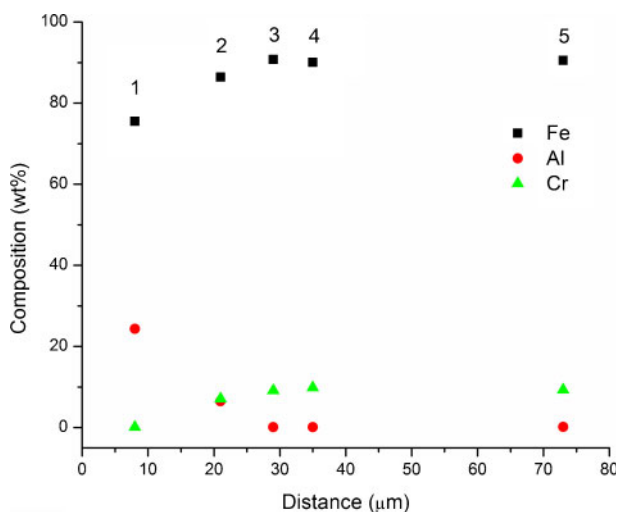
By optical microscopy, the presence of prior austenite grains was clearly revealed, whereas doubts remained regarding the presence of lath martensite within the prior austenite grains. However, the SEM image could prove beyond any doubt the presence of the martensite phase through its effects on the carbide precipitation



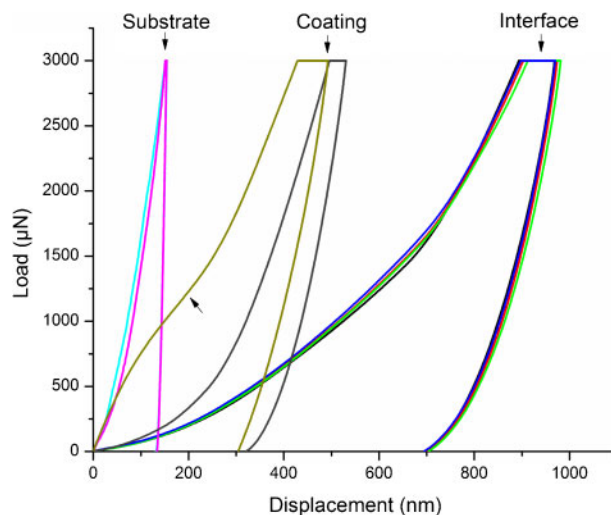
5 Secondary electron cross-section SEM image of aluminide coated 9Cr steel with marked locations of EDX spot analysis

patterns within the grains. In detail, linearly oriented carbides within the prior austenite grains can be taken as an unambiguous sign of martensite lath boundary precipitation.^{23,24} It has been also reported that chromium rich coarse $M_{23}C_6$ type carbides are mostly precipitated on lath boundaries, while fine MX type carbides preferentially form within the laths.

However, major carbon segregation is observed at the aluminide coating/substrate interface, which should have occurred during electrospark processing. Similar observations on carbon segregation at the aluminide/steel interface by HDA process have been reported by Awan and Hasan.²⁵ These authors also reported that carbon segregation promotes martensite formation below the interface. In this work, the presence of carbides with angular morphology indicates the presence of martensite. The local temperature of the substrate during ESD depends essentially on energy and pulse length, usually raising above the melting point of the filler material (for FeAl materials, melting occurs at $\sim 1500^\circ\text{C}$). At the same time, ESD results in rapid cooling rates, which could approach as high as $10^6\text{ }^\circ\text{C s}^{-1}$.^{26,27} The combination of local temperature raise and high cooling rates could well explain the martensite presence right below the interface.



6 Surface to core elemental profiling determined by EDX spot analysis (numbers indicate spot analysis position as from Fig. 5)



7 Load-displacement curves for coating, interface and substrate regions of ESD aluminide coating

Surface to core elemental profiling was determined by EDX spot analysis carried out at the positions marked in Fig. 5. From the EDX results shown in Fig. 6, it appears that the bright interface zone (marked as analysis position 3 in Fig. 5) is deprived of any Al content. Further, the optical micrograph indicates a tinting intensity of this 3–4 μm thick interface (indicated as HAZ in Fig. 2) similar to that of substrate (9Cr steel), while no grains could be visible within this interface zone. This may probably be due to a ferrite layer with a quasi-amorphous structure. The concept of a quasi-amorphous structure for these types of ferritic steels is not totally new. Kayano *et al.*²⁸ and Kohyama *et al.*²⁹ first reported a laser melting process to produce quasi-amorphous ferritic steels in an attempt to reduce hydrogen permeation in structural fusion nuclear materials. In the present case, a 'quasi-amorphous' ferritic steel structure could be justified assuming that the ESD depositions occurred under very high cooling rates. However, further investigation is clearly warranted to confirm the formation of amorphous ferritic layers as a result of ESD processing conditions.

Nanoindentation measurements

Nanoindentation has been carried out using Oliver and Pharr method³⁰ on the cross-section of aluminide coated sample to probe the quasi-amorphous nature of the interface. Figure 3 indicates the locations or zones of the nanoindentation measurements. Owing to the brittle nature of iron aluminides, very low load values (3 mN) were selected so as to achieve reliable data.¹¹ The zones investigated by nanoindentation were (a) coating zone, (b) interface or 'quasi-amorphous ferrite' zone and (c) substrate, as labelled appropriately in Fig. 3. Figure 7 shows typical load-displacement curves of ESD aluminide coating cross-section on areas a, b and c. The measurements conducted in the coating zone ('a') showed some irregularities, i.e. a 'hump' during the loading cycle, as indicated by an arrow in Fig. 7. This is due to the presence of cracks in the coating, which has changed the displacement regime. Such cracks are visible in Fig. 2 and specifically in Fig. 3, where the measurements had been taken. The area of interest, i.e. the interface, showed maximum displacement, indicating a 'soft' phase as compared to the much harder substrate. The average hardness of the soft ferrite interface was measured as

0–116 GPa, while the substrate revealed an average hardness of 2.876 GPa. This confirms that the quasi-amorphous interface (labelled as HAZ in Figs. 2 and 4), while having a composition similar to the substrate, is very soft as compared to the substrate. Some recent work³¹ has reported lower hardness (12–14 GPa) in amorphous Al₂O₃ layers as compared to the crystalline Al₂O₃ (28–31 GPa),³² and this supports the claim of the quasi-amorphous nature of the layer. However, amorphous metals and alloys are typically harder than their crystalline counterparts³³ owing to the lack of slip planes or point defects at grain boundaries. For this reason, amorphous alloys do not show plastic/ductile deformation behaviour. Based on these premises, it is evident that the soft behaviour of the ferrite metallic layer is rather different from the general expected behaviour of amorphous metallic alloys, thus demanding some elucidation. One possibility is the presence of some topological heterogeneity, namely large size atoms that may result in locally variable chemical composition, and this could enhance the mechanical plasticity. This softening behaviour is not totally speculative being already reported in recent literature.³⁴ In our specific case, the softening effect could possibly be produced by the large W atom whose concentration in the 9Cr steel composition is not negligible, being >1 wt-%. However, this hypothesis needs to be investigated further. Another reason could be the absence of carbides, which are segregated at the coating/substrate boundary, as visible in Fig. 4.

Conclusion

From the above microstructural study of ESD aluminide coating, it was observed that carbide segregation took place near the interface during the deposition process. Since such carbides have been reported to precipitate at the grain boundaries, this segregation can be taken as an indication of the increased lath boundary. In this context, the effect of carbide segregation on the mechanical and metallurgical properties as well as tritium permeation needs to be further investigated. Another important observation is that high cooling rates during ESD processing promoted the formation of a soft quasi-amorphous ferrite layer in the HAZ layer at the coating/substrate interface. Since such quasi-amorphous layer does not have a definite grain boundary, its ability to serve as effective hydrogen barriers could be promising and needs to be investigated further. The presence of extensive thermal cracking phenomena in the FeAl coating makes it unsuitable in the present condition, clearly demanding further ESD processing and procedure optimisation for removal of such cracks. Finally, from the results shown in this work, there are good premises to suppose that the quasi-amorphous nature of the HAZ layer could play a decisive role as far as concerned with the functional properties required to the aluminised barrier coatings of blanket modules, such as tritium permeability and liquid metal corrosion resistance. The above mentioned issues are now under intense scrutiny, and further results on these topics will be illustrated in the forthcoming papers.

Acknowledgements

The authors would like to thank Dr V. Badheka of PDP, Gandhinagar, India, for providing the 9Cr

reduced activation steel samples. The work related to XRD and nanoindentation has been carried out at the Department of Metallurgical Engineering and Materials Science, IIT Bombay. The support from these institutions is gratefully acknowledged.

References

1. L. Tan, D. T. Hoelzer, J. T. Busby, M. A. Sokolov and R. L. Klueh: *J. Nucl. Mater.*, 2012, **422**, 45–50.
2. N. Baluc, K. Abe, J. L. Boutard, V. M. Chernov, E. Diegele, S. Jitsukawa, A. Kimura, R. L. Klueh, A. Kohyama, R. J. Kurtz, R. Lasser, H. Matsui, A. Moslang, T. Muroga, G. R. Odette, M. Q. Tran, B. van der Schaaf, Y. Wu, J. Yu and S. J. Zinkle: *Nucl. Fusion*, 2007, **47**, S696–S717.
3. E. Rajendra Kumar, C. Danani, I. Sandeep, Ch. Chakrapani, N. Ravi Pragash, V. Chaudhari, C. Rotti, P. M. Raole, J. Alphonsa and S. P. Deshpande: *Fusion Eng. Des.*, 2008, **83**, 1169–1172.
4. D. L. Smith, J. Konys, T. Muroga and V. Evtikhin: *J. Nucl. Mater.*, 2002, **307–311**, 1314.
5. I. Iordanova, K. S. Forcey and M. Surtchev: *Mater. Sci. Forum*, 2000, **321–324**, 422–427.
6. Y. Ueki, T. Kunugi, N. B. Morley and M. A. Abdou: *Fusion Eng. Des.*, 2010, **85**, 1824–1828.
7. P. Hubberstey and T. Sample: *J. Nucl. Mater.*, 1997, **248**, 140–146.
8. G. Benamati, C. Chabrol, A. Perujo, E. Rigal and H. Glasbrenner: *J. Nucl. Mater.*, 1999, **271–272**, 391–395.
9. T. Shikama, R. Knitter, J. Konys, T. Muroga, K. Tsuchiya, A. Moesslang, H. Kawamura and S. Nagata: *Fusion Eng. Des.*, 2008, **83**, 976–982.
10. W. Krauss, J. Konys, N. Holstein and H. Zimmermann: *J. Nucl. Mater.*, 2011, **417**, (1–3), 1233–1236.
11. S. Frangini, S. Loreti and A. Masci: *J. Fuel Cell Sci. Technol.*, 2005, **2**, 60–64.
12. A. Mignone, S. Frangini, A. la Barbera and O. Tassa: *Corros. Sci.*, 1998, **40**, (8), 1331–1347.
13. H. G. Yang, Q. Zhan, W. W. Zhao, X. M. Yuan, Y. Hu and Z. B. Han: *J. Nucl. Mater.*, 2011, **417**, (1–3), 1237–1240.
14. B. A. Pint and K. L. More: *J. Nucl. Mater.*, 2008, **376**, 108–113.
15. S. Frangini and A. Masci: *Surf. Coat. Technol.*, 2010, **204**, 2613–2623.
16. 'ASM metals handbook', Vol. 9, 'Metallography and microstructures', 9th edn; 1999, Ohio, ASM International.
17. H. Glasbrenner and O. Wedemeyer: *J. Nucl. Mater.*, 1998, **257**, 274–281.
18. R. L. Klueh and D. R. Harries: 'High chromium ferritic and martensitic steels for nuclear applications', Monograph 3, 30–31; 2001, West Conshohocken, PA, ASTM Publication.
19. J. L. Smialek, J. Doychack and D. J. Gaydos: *Oxid. Met.*, 1990, **34**, 259–275.
20. B. A. Pint, Y. Zhang, P. F. Tortorelli, J. A. Haynes and I. G. Wright: *Mater. High Temp.*, 2001, **18**, 185–192.
21. N. Radek and B. Antoszewski: *Mater. Eng.*, 2005, **4**, 13–15.
22. N. Radek and K. Bartkowiak: *Phys. Proc.*, 2010, **5**, 417–423.
23. S. Saroja, A. Dasgupta, R. Divakar, S. Raju, E. Mohandas, M. Vijayalakshmi, K. Bhanu Shankara Rao and B. Raj: *J. Nucl. Mater.*, 2011, **409**, (2), 131–139.
24. B. Raj, K. Bhanu Shankara Rao and A. K. Bhaduri: *Fusion Eng. Des.*, 2010, **85**, 1460–1468.
25. G. H. Awan and F. ul Hasan: *Mater. Sci. Eng. A*, 2008, **A472**, 157–165.
26. S. Cadney and M. Brochu: *Intermetallics*, 2008, **16**, 518–523.
27. Y. Xie and M. Wang: *Surf. Coat. Technol.*, 2006, **201**, 691–698.
28. H. Kayano, K. Sugauma, M. Narui, S. Suzuki and H. Kusanagi: *J. Nucl. Mater.*, 1979, **85–86**, 925.
29. A. Kohyama, Y. Kohno, K. Asakura and H. Kayano: *J. Nucl. Mater.*, 1994, **212–215**, 684–689.
30. W. C. Oliver and G. M. Pharr: *J. Mater. Res.*, 1992, **7**, 1564.
31. N. G. Chechenin, J. Bottiger and J. P. Krog: *Thin Solid Films*, 1995, **261**, 219–227.
32. Q. Li, Y.-H. Yu, C. Singh Bhatia, L. D. Marks, S. C. Lee and Y. W. Chung: *J. Vac. Sci. Technol. A*, 2000, **18A**, (5), 2333–2338.
33. X. J. Gu, S. Joseph Poon, G. J. Shiflet and M. Widom: *Acta Mater.*, 2008, **56**, 88–94.
34. N. Zheng, R. T. Qu, S. Pauly, M. Calin, T. Gemming, Z. F. Zhang and J. Eckert: *Appl. Phys. Lett.*, 2012, **100**, 141901.